

High-Rate Performance All-Solid-State Li-SeS₂ Battery with Selenium sulphide/three-dimensional graphene as cathode material

Wenyan Li¹, Fangchao Liu^{1,*}, Zhongli Shen¹, Han Hu¹ and Zhengwen Fu²

¹ School of Materials Engineering, Shanghai University of Engineering Science, Shanghai 201600, P.R China;

² Department of Chemistry, Shanghai Key Laboratory of Molecular Catalysis and Innovative Materials, Fudan University, Shanghai, 200433, P.R China.

*E-mail: 84309286@qq.com

Received: 13 March 2021 / Accepted: 6 May 2021 / Published: 31 May 2021

Selenium sulfide (SeS₂) shows attractive advantages of high capacity for lithium storage. Here, a free-standing ultra-high dispersion Selenium sulfide three-dimensional graphene (SeS₂-3DG) was synthesized and used as a cathode material in all-solid-state Lithium-Selenium sulfide (Li-SeS₂) batteries for enhancing rate performance and utilization of SeS₂. SeS₂-3DG achieved the utilization rate of 103% with capacity of 1,163 mAh g⁻¹ and remained 538.56 mAh g⁻¹ after 20 cycles under 1/2C. It should be noted that SeS₂-3DG exhibited outstanding rate performance, which discharged under 7C with capacity as high as 990 mAh g⁻¹. Due to the high utilization rate of SeS₂, charge and discharge products of Li-SeS₂ batteries were observed by high-resolution transmission electron microscopy (HRTEM) and selected area electron diffraction (SAED). The mechanism of lithium sulfide (Li₂S)/ Lithium selenide (Li₂Se) ↔ SeS₂ was confirmed.

Keywords: Ultra-high dispersion, All-solid-state, Li-SeS₂ batteries, Charge and discharge products, High utilization

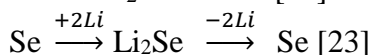
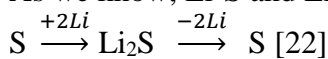
1. INTRODUCTION

In recent years, rechargeable batteries with high energy density, high rate performance and safety have received extensive attention due to potential applications in electric vehicles and energy storage systems.[1-4] The energy density is mainly limited by the cathode material used in lithium-ion batteries.[5] With superior theoretical capacity (1,672 mAh·g⁻¹), lithium-sulfur (Li-S) batteries possess energy density as high as 2,600 Wh·kg⁻¹, 2–5 times of that of conventional Li ion cells.[6-8] The

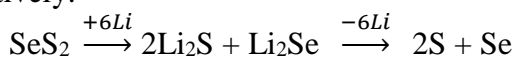
problems of low-conductivity of S and Li_2S limit the practical application of Li-S battery.[9] Selenium (Se), as a homologue of S, has been studied as an alternative cathode for lithium batteries due to its high electrochemical activity.[10, 11] However, Se shows higher cost and lower gravimetric capacity than S. In order to overcome the aforementioned disadvantages of S and Se, S/Se solid solution in the carbon matrix has been explored in lithium batteries.[12-15]

Selenium sulfide (SeS_2) has the advantage of high gravimetric capacity ($1,124 \text{ mAh}\cdot\text{g}^{-1}$), combining high capacity of S and high electrochemical activity of Se.[15-17] However, it still suffers from large volume changes and shuttle effect during the charge/discharge process.[18] All-solid-state batteries can effectively alleviate the shuttle effect and safety issues of liquid batteries.[19-21] Sun et al. reported all-solid-state battery of $\text{SeS}_2/\text{Li}_{10}\text{GeP}_2\text{S}_{12}\text{-Li}_3\text{PS}_4/\text{Li}$ delivered the 1st discharge capacity of $1100 \text{ mAh}\cdot\text{g}^{-1}$ under 50mA/g and long cycling life for 100 cycles.[17] The mechanism of the battery has not yet studied, which may be related to solid electrolyte containing Li_2S . Cui et al. argue that Li_2Se and Li_2S are the discharge products of Li- SeS_2 cells. It is only the existence of Se as the charge product without any information of S.[8] Complete charge and discharge products of Li- SeS_2 batteries have not been fully studied.

As we know, Li-S and Li-Se batteries operate based upon the electrochemical reaction:



Li- SeS_2 batteries may have two competing charge reaction mechanisms to generate S/Se or SeS_2 , respectively:



In this work, we design and propose a suitable Li- SeS_2 battery and research complete charge and discharge products. Free-standing ultra-high dispersion SeS_2 -3DG soaking liquefied small molecule complex solid electrolyte LiHFN-0.5LiI (SMC) is used to assemble all-solid-state Li- SeS_2 battery. Li- SeS_2 battery delivers the first discharge capacity of $1,163 \text{ mAh}\cdot\text{g}^{-1}$ under $1/2\text{C}$ and obtains $538.59 \text{ mAh}\cdot\text{g}^{-1}$ after 20 cycles. Li- SeS_2 battery shows outstanding rate performance with capacity as high as $990 \text{ mAh}\cdot\text{g}^{-1}$ under 7C . Mixed $\text{Li}_2\text{S}/\text{Li}_2\text{Se}$ and SeS_2 are observed by HRTEM and SAED as the discharge and charge products under $1/2\text{C}$ cycling.

2. EXPERIMENTAL

2.1. Materials

Graphite, selenium, powder and sublimed sulfur were purchased from Sinopharm Chemical Reagent Co. Ltd. Nitrate of potash, lithium iodide, concentrated sulfuric acid, concentrated hydrochloric acid and potassium permanganate were purchased from Shanghai Titan Co., Ltd. Sodium sulfide nonahydrate, hydroiodic acid, hydrogen peroxide, vitamin C, acetonitrile and lithium carbonate tablets were purchased from Afa Aisa (China) Chemical Co., Ltd. Three—hydroxypropionitrile was purchased from Aladdin Reagents Co., Ltd. Ultrapure water ($18.2 \text{ M}\Omega \text{ cm}$) was used in all of experiments.

2.2. Synthesis of SeS₂-3DG Foam and SMC

Graphene oxide (GO) dispersion was synthesized by an improved Hummers' method.[24] SeS₂-3DG was prepared by a simple in-situ synthesis method. SeS₂ was 60wt.% content of SeS₂-3DG. Under acidic conditions, 5.6 mL 3mg/mL of GO dispersion, 4.4 mL 0.056mmol/mL of Na₂S solution and S/Se powder were mixed and heated at 110°C for 75 minutes. After cooling and freeze-drying for 12 hours, SeS₂-3DG was obtained. SMC was prepared in our previous work.[25]

2.3. Assembly of Batteries

The structure of all-solid-state Li/SMC/SeS₂-3DG battery was as follows: the anode was a lithium sheet (99.999% purity), the cathode was a dry and electrolyte-filled SeS₂-3DG and the separator was a 25µm glass fiber. The lithium sheet was pressed onto the separator fiber soaked in SMC with SeS₂-3DG to assemble the battery in a water-less glove box.

2.4. Characterization

X-ray diffraction (XRD) was used to test rGO and SeS₂-3DG with Cu Kα radiation in the 2θ range of 5° to 100° (Panalytical X'Pert X-ray diffractometer, Netherlands). The Thermogravimetric (TG) curve atmosphere of SeS₂-3DG was measured from 25°C to 700°C under the N₂ atmosphere. Scanning electron microscopy (SEM) and energy dispersive spectrometer (EDS) (VEGA3 TESCAN) spectroscopy were used to study the morphology and microstructure of SeS₂-3DG. HRTEM and SAED (JEOL 2100F, 200kV) modes were obtained for research. X-ray photoelectron spectroscopy (XPS) (ThermoFisher, Escalab 250Xi) spectroscopy was performed with an Al target at a base pressure of 10⁻⁷ Pa.

2.5 Electrochemical Measurement

The Land CT-2001A Battery Tester (Wuhan, China) was used for constant current discharge/charge test at various current densities. The current densities and capacities were calculated based on the gross mass of active material SeS₂ in SeS₂-3DG. Both cyclic voltammetry (CV) and electrochemical impedance spectroscopy (EIS) were evaluated on a CHI 660C (Chen Hua Co., China), with scanning speeds of 0.02 mV/s, 0.05 mV/s and 0.07 mV/s and a frequency range of 0.01~10⁶ Hz. Li/SMC/SeS₂-3DG batteries were used to evaluate all electrochemical measurements.

3. RESULTS AND DISCUSSION

Fig. 1. illustrates schematic of discharge and charge products based on free-standing ultra-high dispersion SeS₂-3DG electrode. Typically, Li₂S generates S and Li₂Se generates Se in the charge process of Li-S and Li-Se batteries:



Therefore, as illustrated in Fig. 1. (top-right), charge process of fully discharged Li-SeS₂ batteries can be expressed as:

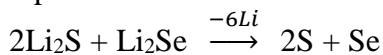


Fig. 1. (bottom-right) shows another process containing different types of discharge and charge products:



Mixed Li₂S/Li₂Se is generated from highly dispersed SeS₂ on the large surface area of 3D-graphene without the enrichment and agglomeration of Li₂S or Li₂Se. Instead of S and Se, SeS₂ could be regenerated in the charge process of mixed Li₂S/Li₂Se. Test and analysis of the charge and discharge products can provide basic and important information about the mechanism of Li-SeS₂ batteries.

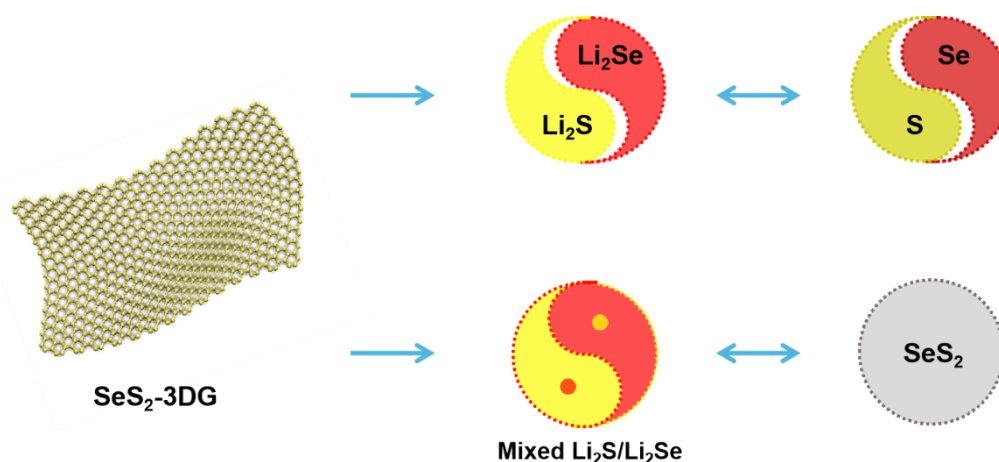


Figure 1. Schematic of discharge and charge products based on SeS₂-3DG.

As shown in Fig. 2a, Raman peaks show two broad carbon peaks at 1,340 cm⁻¹ and 1,583 cm⁻¹, representing the disordered graphite (D band) and crystalline graphite (G band), respectively. [37] The intensity ratio of D to G band is I_D/I_G = 1.30, which indicates the graphitization degree of carbon. The XRD patterns of 60%SeS₂-3DG and Se_{2.57}S_{5.43}(JCPDS NO.01-073-2267)[17] are illustrated in Fig. 2b. In the XRD pattern of the 60%SeS₂-3DG, the diffraction peak of graphene was observed. No obvious crystalline peak of SeS₂ was found, indicating that SeS₂ was oxidized into an amorphous form by GO.[26] The weight loss of SeS₂-3DG at 150°C-700°C shown in TG curve should be attributed to SeS₂ sublimation.[12] The weight loss indicates SeS₂ is almost 60% in SeS₂-3DG (Fig. 2c). Fig. 2d shows C, O, S and Se are four main elements of SeS₂-3DG. The high-resolution C 1s spectrum of SeS₂-3DG in Fig. 2e can be fitted to four peaks at 283.8 eV, 285.4 eV, and 287.8 eV and assigned to C=C, C-C or C-S and C=O bonds, respectively.[38] The graphene oxide has been well reduced because we observed that the peaks of the C-O and C=O bonds were relatively weak. Moreover, Fig. 2f. shows the S 2p and Se 3p XPS spectrum, confirming the existence of S-Se banding in SeS₂-3DG.[10] FESEM image of SeS₂-3DG in Fig. 2g. shows that no SeS₂ particles were observed on 3D graphene[27].

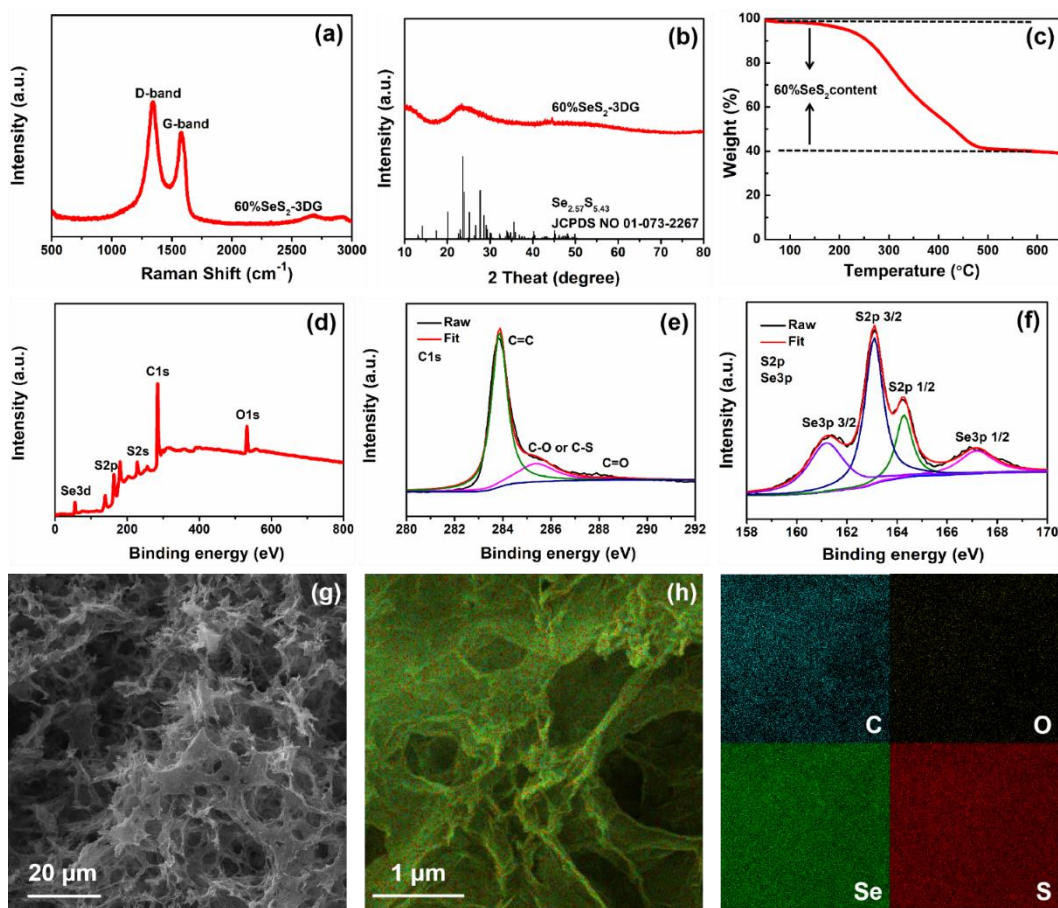


Figure 2. (a) Raman, (b) XRD, (c) TG, (d-f) XPS, (g) FESEM and (h) EDS mapping results of 60%SeS₂-3DG.

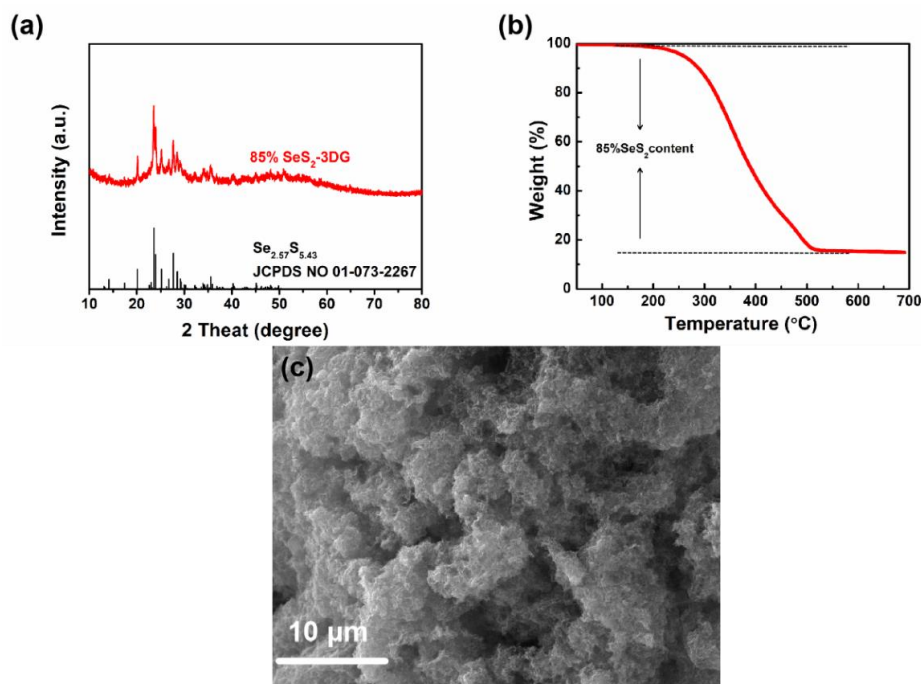


Figure 3. (a) XRD (b)TG and (c) FESEM images of 85%SeS₂-3DG.

The cross-linked porous structure provides a good conductive network[28] and can be readily infiltrated by the liquefied SMC solid electrolyte.[29, 30] In Fig. 2h, the EDS images indicate that C, O, S and Se are four main elements of SeS₂-3DG, which is consistent with what the XPS showed. What's more, EDS images show uniform Se and S on the surface of SeS₂-3DG, suggesting highly dispersion of SeS₂ on 3D-graphene.

As shown in Fig. 3a, the X-ray diffraction of 85%SeS₂-3DG and Se_{2.57}S_{5.43}(JCPDS NO.01-073-2267)[39]. SeS₂ was successfully prepared by in-situ method. Fig. 3b illustrates the weight loss of SeS₂-3DG, implying that SeS₂ loading were about 85%. SEM image of 85%SeS₂-3DG is shown in Fig. 3c.

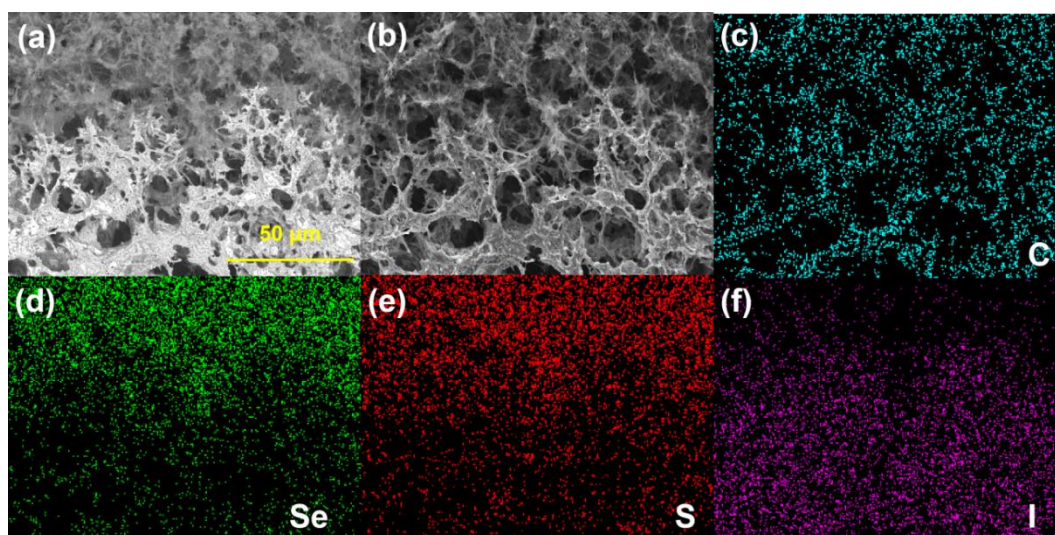


Figure 4 (a) BSEM, (b) SEM and (c-f) EDS mapping results of SeS₂-3DG @ SMC.

Fig. 4a-4b shows the SeS₂-3DG @ SMC composite electrode material was obtained by integrating a moderate SMC and SeS₂-3DG. It was observed that a layer of SMC film covered the SeS₂-3DG and was distributed on the inside and outside of the wrinkled graphene. Fig. 4c-4f presents the EDS mapping results for C, Se, S and I in SeS₂-3DG@SMC composite electrode, respectively. These results indicate that SMC is closely anchored on SeS₂-3DG, and that they are in complete contact.

Discharge and charge products were analyzed through HRTEM and SAED.[31] Fig. 5a-5c show that ~25 nm discharge products are tightly anchored on 3D-graphene, with Se and S uniformly distributed. The HRTEM image with clear lattice fringe of discharge products are shown in Fig. 5d. (111) and (220) plane of Li₂S can be confirmed with 0.330 nm and 0.202 nm lattice spacing (PDF#26-1188;Li₂S),[32] and (220) plane of Li₂Se can be confirmed with 0.212 nm lattice spacing (PDF#23-0072;Li₂Se).[33] In the inset of Fig. 5d. (top-left), SAED image illustrates (511), (222), (311) and (220) planes of Li₂S (PDF#26-1188; Li₂S) and (511), (222) and (220) planes of Li₂Se (PDF#23-0072; Li₂Se).

Fig. 5e-5g indicates that ~20 nm charge products with Se and S are uniformly distributed. In Fig. 5h, (121), (230) and (-132) planes of SeS₂ can be confirmed with 0.350, 0.273 and 0.317 nm lattice spacing (PDF#47-1481; SeS₂). [34] SAED spectra illustrates (042), (230) and (-113) planes of SeS₂

(PDF#47-1481; SeS_2). Charge product SeS_2 is generated from fully discharge product of mixed $\text{Li}_2\text{S}/\text{Li}_2\text{Se}$, which confirms the mechanism of mixed $\text{Li}_2\text{S}/\text{Li}_2\text{Se} \leftrightarrow \text{SeS}_2$.

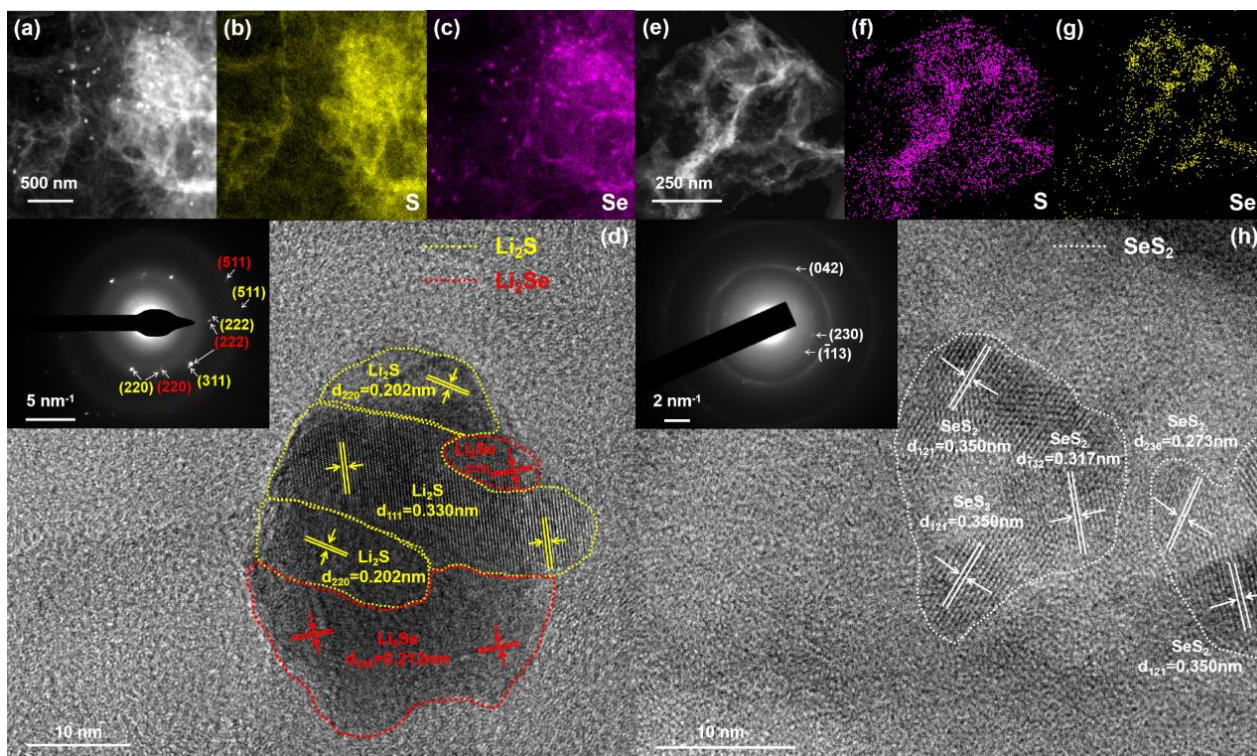


Figure 5. STEM, HRTEM, EDS and SAED images for (a-d) discharge and (e-h) charge products of SeS_2 -3DG electrode.

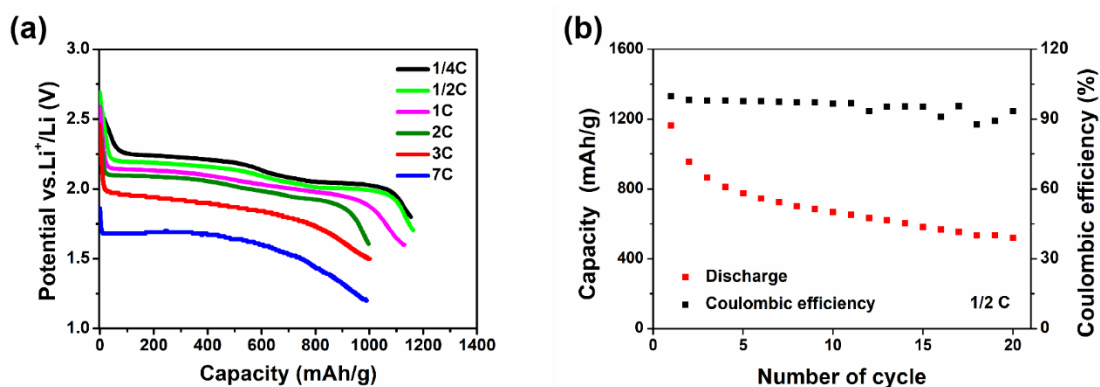


Figure 6. Li/SMC/60% SeS_2 -3DG batteries of (a) rate and (b) cycle performance at 45 °C.

Li/SMC/60% SeS_2 -3DG battery was assembled and tested to evaluate the electrochemical characterizations of 60% SeS_2 -3DG at 45°C. Fig. 6a. exhibits the discharge curves of Li/SMC/60% SeS_2 -3DG batteries at various C-rates. The batteries deliver remarkable the 1st discharge capacity of 1,154 mAh g^{-1} , 1,163 mAh g^{-1} , and 1,130 mAh g^{-1} up to 100% utilization rate under 1/4C, 1/2C and 1C respectively (1C = 1125 mAh g^{-1}), and can attain more than 88% utilization rate under 2C, 3C and 7C

(especially 990 mAh g⁻¹ under 7C). Such high rate performance benefits from efficient activation of 3D-graphene and liquefied SMC by ultra-high dispersion SeS₂. [35] Fig. 6b. shows discharge capacity and coulombic efficiency of Li/ SMC/ 60%SeS₂-3DG battery from 1.7 to 2.7 V under 1/2C. The capacity remained to be 955 mAh g⁻¹ after the 2nd discharge and was about 538 mAh g⁻¹ after 20 cycles with the coulombic efficiency of around 95%.

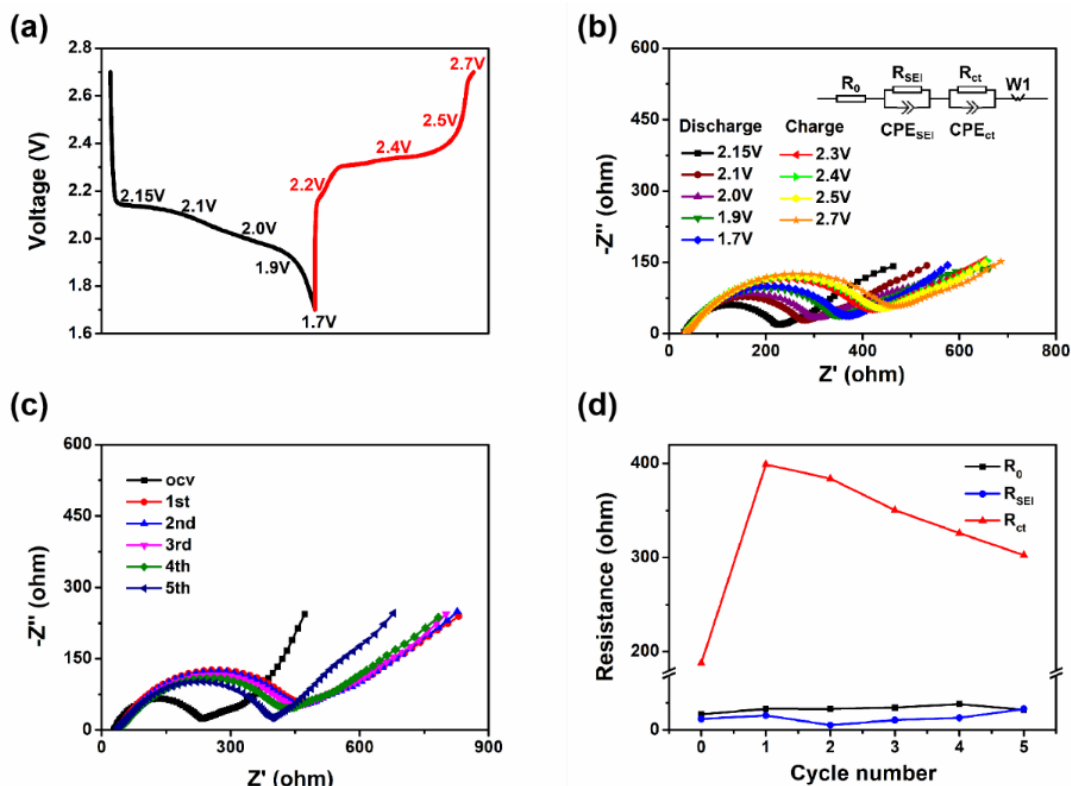


Figure 7. EIS spectras of battery (a-b) at different voltages during discharge and charge, (c) EIS spectras before cycling and 1st to 5th cycle, (d) Fitting parameters of EIS plots in (c) before cycling and 1st to 5th cycle.

EIS analysis can effectively provide the change and discharge of battery resistance, so it was used to investigate the attenuation and reaction mechanism of the Li-SeS₂ battery. Fig.7a-7b illustrates that the EIS of the Li-SeS₂ battery at different depths of charge/discharge were carried out individually under 1/2C. The resistance of the electrolyte (R_0), SMC/SeS₂-3DG interface (R_{SEI}) and charge-transfer in SMC (R_{ct}) was at high, medium and low frequency, respectively (the equivalent circuit as inset Fig. 7b). [36] The impedance of the 60%SeS₂-3DG composite electrode in the fully charge state after the cycle from 1st to 5th was detected under 1/2C (Fig. 7c). Fitting parameters of EIS plots are shown in Table S1-S2. During discharging, R_{ct} increased from 153.7 (2.15 V) to 327 Ω (1.7 V), with the generation of Li₂S/Li₂Se. Charge produce SeS₂ could cause R_{ct} increased to 392 Ω (2.7 V). In the first five cycles of the battery, R_{ct} decreased from 399 (1st) to 302.6 Ω (5th), which was caused by the reversible conversion of Li₂S/Li₂Se and SeS₂.

Table 1. Fitting values of impedance parameters of battery during discharge and charge.

	Voltage (V)	$R_0(\Omega)$	$R_{SEI}(\Omega)$	$R_{ct}(\Omega)$
Discharge	2.15	32.36	29.59	153.7
	2.1	29.65	21.34	198.1
	2.0	27.29	23.34	262.7
	1.9	26.93	12.21	279.8
	1.8	26.4	10.22	297
	1.7	21.26	14.63	327
Charge	2.3	24.95	9.45	330.7
	2.4	33.56	28.04	296.8
	2.5	34.48	32.93	302.6
	2.7	35.83	36.15	392

Table 2. Fitting values of impedance

	$R_0(\Omega)$	$R_{SEI}(\Omega)$	$R_{ct}(\Omega)$
Before cycling	28.83	20.31	187.9
1st cycle	38.86	26.75	399
2nd cycle	38.62	9.16	383.7
3rd cycle	41.09	18.23	350.3
4th cycle	47.63	22.44	325.9
5th cycle	36.87	38.72	302.6

When medium rate was increased to 1C, the coulombic efficiency seriously dropped to 60%-80%, and when it continued to be increased to 2C, the coulomb efficiency stabilized around 100% (Fig.8a). Similarly, charge/discharge rate affected the performance of the battery, as shown in CV analysis in Fig. 8b-8d. CV diagrams of low and high scan rates (0.02mV/s and 0.07mV/s) did not change significantly. Under medium scan rate, new charge peak appeared obviously at 2.22V, so $\text{Li}_2\text{Se} \leftrightarrow \text{Se}$ was likely to generate Se.[26] The attenuation of Li-SeS₂ battery may be related to the competitive reaction mechanism of $2\text{Li}_2\text{S} + \text{Li}_2\text{Se} \leftrightarrow 2\text{S} + \text{Se}$. The Li-SeS₂ battery was designed and controlled based on SeS₂ as a reversible active material with the mechanism of $\text{Li}_2\text{S}/\text{Li}_2\text{Se} \leftrightarrow \text{SeS}_2$, exhibiting important practical value.

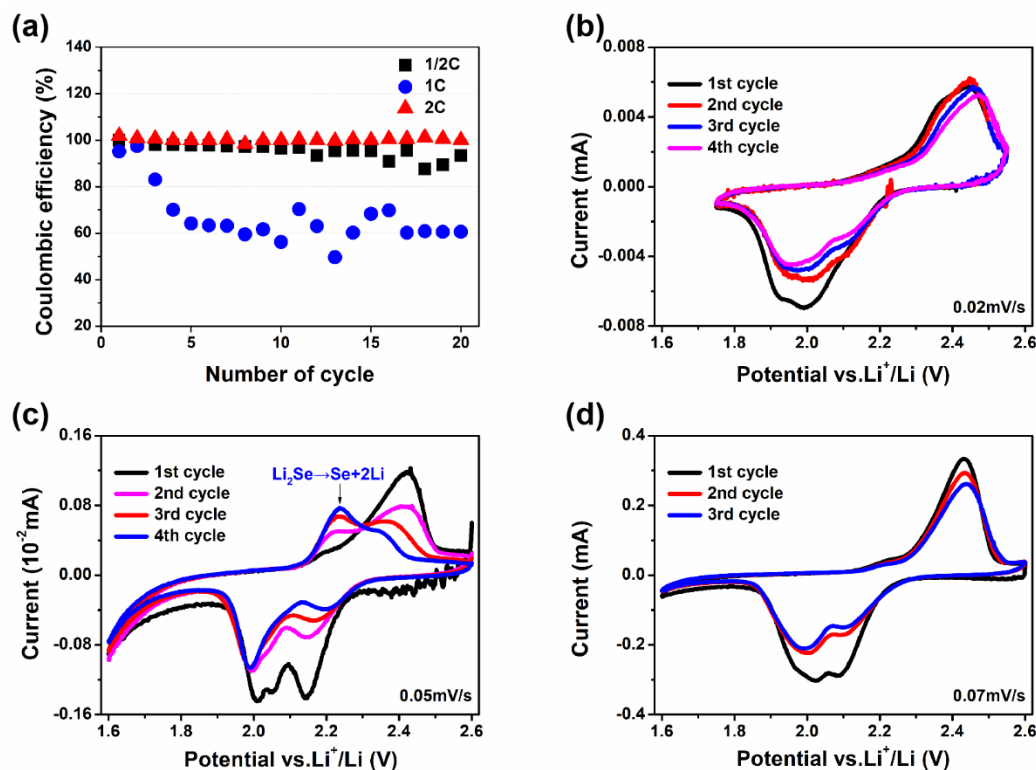


Figure 8. (a). Coulomb efficiency-cycle numbers under different C-rate, (b-d) CV curves of different scan rates.

4. CONCLUSION

By HRTEM and SAED analysis of discharge and charge products of ultra-high dispersion SeS_2 -3DG cathode under 1/2C, recycling mechanism of $\text{Li}_2\text{Se}/\text{Li}_2\text{S} \leftrightarrow \text{SeS}_2$ was confirmed. We observed for the first time, mixed $\text{Li}_2\text{S}/\text{Li}_2\text{Se}$ and SeS_2 were the discharge and charge products of all-solid-state Li-Se S_2 batteries. Benefiting from the distinct advantages of highly activated SeS_2 , Li-Se S_2 battery exhibited 7 C high-rate performance of 990mAh g^{-1} and reached 100% utilization of SeS_2 under 1/2 C. Under different rates, recycling mechanism of $2\text{Li}_2\text{S} + \text{Li}_2\text{Se} \leftrightarrow 2\text{S} + \text{Se}$ was proposed to be quite different from that of mixed $\text{Li}_2\text{S}/\text{Li}_2\text{Se} \leftrightarrow \text{SeS}_2$. Study of cycling products can provide basic and meaningful information for further designing Se/S-based materials to improve lithium batteries.

References

1. S. Liu, X. Xia, S. Deng, D. Xie, Z. Yao, L. Zhang, S. Zhang, X. Wang, J. Tu, *Adv Mater*, 31 (2019) e1806470.
2. S.Z. Zhang, X.H. Xia, D. Xie, R.C. Xu, Y.J. Xu, Y. Xia, J.B. Wu, Z.J. Yao, X.L. Wang, J.P. Tu, *Journal of Power Sources*, 409 (2019) 31-37.
3. Z. Sun, J. Zhang, L. Yin, G. Hu, R. Fang, H.M. Cheng, F. Li, *Nat Commun*, 8 (2017) 14627.
4. C. Wang, Z. Guo, W. Shen, A. Zhang, Q. Xu, H. Liu, Y. Wang, *Journal of Materials Chemistry A*, 3 (2015) 6064-6072.
5. J.M. Buriak, C. Toro, *Chemistry of Materials*, 30 (2018) 559-560.
6. X. Ji, K.T. Lee, L.F. Nazar, *Nat Mater*, 8 (2009) 500-506.

7. B. Zhang, X. Qin, G.R. Li, X.P. Gao, *Energy & Environmental Science*, 3 (2010) 1531-1537.
8. Y. Cui, A. Abouimrane, J. Lu, T. Bolin, Y. Ren, W. Weng, C. Sun, V.A. Maroni, S.M. Heald, K. Amine, *J Am Chem Soc*, 135 (2013) 8047-8056.
9. Y. Yao, R. Xu, M. Chen, X. Cheng, S. Zeng, D. Li, X. Zhou, X. Wu, Y. Yu, *ACS Nano*, 13 (2019) 4695-4704.
10. J. Hu, H. Zhong, X. Yan, L. Zhang, *Applied Surface Science*, 457 (2018) 705-711.
11. J.T. Lee, H. Kim, M. Oschatz, D.-C. Lee, F. Wu, H.-T. Lin, B. Zdyrko, W.I. Cho, S. Kaskel, G. Yushin, *Advanced Energy Materials*, 5 (2015) 1400981.
12. J. Hu, Y. Ren, L. Zhang, *Journal of Power Sources*, 455 (2020) 227955.
13. F. Sun, H. Cheng, J. Chen, N. Zheng, Y. Li, J. Shi, *ACS Nano*, 10 (2016) 8289-8298.
14. G.L. Xu, T. Ma, C.J. Sun, C. Luo, L. Cheng, Y. Ren, S.M. Heald, C. Wang, L. Curtiss, J. Wen, D.J. Miller, T. Li, X. Zuo, V. Petkov, Z. Chen, K. Amine, *Nano Lett*, 16 (2016) 2663-2673.
15. J. Zhang, Z. Li, X.W.D. Lou, *Angew Chem Int Ed Engl*, 56 (2017) 14107-14112.
16. A. Abouimrane, D. Dambournet, K.W. Chapman, P.J. Chupas, W. Weng, K. Amine, *J Am Chem Soc*, 134 (2012) 4505-4508.
17. X. Li, J. Liang, J. Luo, C. Wang, X. Li, Q. Sun, R. Li, L. Zhang, R. Yang, S. Lu, H. Huang, X. Sun, *Adv Mater*, 31 (2019) e1808100.
18. H. Zhang, L. Zhou, X. Huang, H. Song, C. Yu, *Nano Research*, 9 (2016) 3725-3734.
19. X. Tao, Y. Liu, W. Liu, G. Zhou, J. Zhao, D. Lin, C. Zu, O. Sheng, W. Zhang, H.-W. Lee, Y. Cui, *Nano Letters*, 17 (2017) 2967-2972.
20. S. Urbonaite, T. Poux, P. Novák, *Advanced Energy Materials*, 5 (2015) 1500118.
21. C. Wang, Y. Zhao, Q. Sun, X. Li, Y. Liu, J. Liang, X. Li, X. Lin, R. Li, K.R. Adair, L. Zhang, R. Yang, S. Lu, X. Sun, *Nano Energy*, 53 (2018) 168-174.
22. L. Li, C. Chen, A. Yu, *Science China*, 60 (2017) 1402-1412.
23. R. Mukkabila, S. Deshagani, P. Meduri, M. Deep, P. Ghosal, *ACS Energy Letters*, (2017) 1288-1295.
24. D.C. Marcano, D.V. Kosynkin, J.M. Berlin, A. Sinitskii, Z. Sun, A. Slesarev, L.B. Alemany, W. Lu, J.M. Tour, *Acs Nano*, 4 (2010) 4806.
25. R. Zhu, F. Liu, W. Li, Z. Fu, *ChemistrySelect*, 5 (2020) 9701-9708.
26. Z. Zhang, S. Jiang, Y. Lai, J. Li, J. Song, J. Li, *Journal of Power Sources*, 284 (2015) 95-102.
27. K. Wang, L. Shi, M. Wang, H. Yang, Z. Liu, H. Peng, *Acta Physico-Chimica Sinica*, 35 (2019) 1112-1118.
28. Y. Zhong, X. Xia, S. Deng, D. Xie, S. Shen, K. Zhang, W. Guo, X. Wang, J. Tu, *Advanced Materials*, 30 (2018) 1805165.
29. Q. Zhang, H. Wan, G. Liu, Z. Ding, J.P. Mwizerwa, X. Yao, *Nano Energy*, 57 (2019) 771-782.
30. A. Zw, B. Cx, C.A. Lu, S.B. Jian, A. Wl, B. Sh, J.A. Yong, B. Zc, Z.B. Bing, *Electrochimica Acta*, 312 (2019) 282-290.
31. X.-L. Li, S. Bai, X.-Y. Yue, D. Chen, Q.-Q. Qiu, Y. Song, X.-J. Wu, Y.-N. Zhou, *Journal of Alloys and Compounds*, 838 (2020) 155613.
32. P.T. Cunningham, S.A. Johnson, E.J. Cairns, *Journal of The Electrochemical Society*, 118 (1972)1941.
33. E. Zintl, A. Harder, B. Dauth, *Ztschrift fr Elektrochemie, Berichte der Bunsengesellschaft für physikalische Chemie*, 40 (1934) 588-593.
34. M.F. Kotkata, S.A. Nouh, L. Farkas, M.M. Radwan, *Journal of Materials Science*, 27 (1992) 1785-1794.
35. X. Yao, H. Ning, F. Han, Z. Qiang, H. Wan, J.P. Mwizerwa, C. Wang, X. Xu, *Advanced Energy Materials*, 7 (2017) 9231-9239.
36. X. Li, J. Liang, K. Zhang, Z. Hou, W. Zhang, Y. Zhu, Y. Qian, *Energy & Environmental Science*, 8 (2015) 3181-3186

37. Y. Qu, Z. Zhang, S. Jiang, X. Wang, Y. Lai, Y. Liu, J. Li, *Journal of Materials Chemistry A*, 2 (2014) 12255-12261.
38. J. Hu, H. Zhong, X. Yan, L. Zhang, *Applied Surface Science*, 457 (2018) 705-711.
39. X. Li, J. Liang, J. Luo, C. Wang, X. Li, Q. Sun, R. Li, L. Zhang, R. Yang, S. Lu, H. Huang, X. Sun, *Adv Mater*, 31 (2019) e1808100.

© 2021 The Authors. Published by ESG (www.electrochemsci.org). This article is an open access article distributed under the terms and conditions of the Creative Commons Attribution license (<http://creativecommons.org/licenses/by/4.0/>).